

Pressure-induced unusual metallic state in EuNiO_3

Hisao Kobayashi* and Shugo Ikeda

*Graduate School of Material Science and Center for
Novel Material Science under Multi-Extreme Conditions,
University of Hyogo, Koto Hyogo 678-1297, JAPAN*

Yoshitaka Yoda, Naohisa Hirao, and Yasuo Ohishi

Japan Synchrotron Radiation Institute, Hyogo 679-5198, JAPAN

J. A. Alonso and M. J. Martinez-Lope

*Instituto de Ciencia de Materiales de Madrid,
CSIC, Cantoblanco, E-28049 Madrid, SPAIN*

R. Lengsdorf, D. I. Khomskii, and M. M. Abd-Elmeguid

*II. Physikalisches Institut, Universität zu Köln,
Zùlpicher Straße 77, 50937 Köln, GERMANY*

(Dated: May 19, 2015)

Abstract

The perovskite antiferromagnetic ($T_N \sim 220$ K) insulator EuNiO_3 undergoes at ambient pressure a metal-to-insulator transition at $T_{\text{MI}} = 460$ K which is associated with a simultaneous orthorhombic-to-monoclinic distortion, leading to charge disproportionation. We have investigated the change of the structural and magnetic properties of EuNiO_3 with pressure (up to ~ 20 GPa) across its quantum critical point (QCP) using low-temperature synchrotron angle-resolved x-ray diffraction and ^{151}Eu nuclear forward scattering of synchrotron radiation, respectively. With increasing pressure we find that after a small increase of T_N ($p \leq 2$ GPa) and the induced magnetic hyperfine field B_{hf} at the ^{151}Eu nucleus ($p \leq 9.7$ GPa), both T_N and B_{hf} are strongly reduced and finally disappear at $p_c \cong 10.5$ GPa, indicating a magnetic QCP at p_c . The analysis of the structural parameters up to 10.5 GPa reveals no change of the lattice symmetry within the experimental resolution. Since the pressure-induced insulator-to-metal transition occurs at $p_{\text{IM}} \cong 6$ GPa, this result implies the existence of an antiferromagnetic metallic state between 6 and 10.5 GPa. We further show from the analysis of the reported high pressure electrical resistance data on EuNiO_3 at low-temperatures that in the vicinity of the QCP the system behaves as non-Fermi-liquid, with the resistance changing as T^n , with $n=1.6$, whereas it becomes a normal Fermi-liquid, $n = 2$, for pressures above ~ 15 GPa. On the basis of the obtained data a magnetic phase diagram in the (p , T) space is suggested.

PACS numbers: 71.30.+h, 62.50.-p, 71.28.+d, 76.80.+y

* kobayash@sci.u-hyogo.ac.jp

I. INTRODUCTION

The study of magnetic quantum transitions in strongly correlated electron systems has been the subject of continuous interest due to the observation of novel ground states near/at the magnetic-to-nonmagnetic transition leading to quantum critical point (QCP). Known examples are heavy-fermion metals where non-Fermi-liquid (NFL) phases (e.g. $\text{CeCu}_{6-x}\text{Au}_x$ [1, 2] and YbRh_2Si_2 [3]) and unconventional superconductivity (e.g. CePd_2Si_2 [4] and UGe_2 [5]) appear.

Another promising but different class of systems for such studies are strongly correlated transition metal oxides [6] (e.g. RMO_3 perovskites, R = rare earth ion; M = transition metal). The key aspect of these materials is that the interplay between spin, charge, and orbital degrees of freedom leads to the existence of several competing phases and in turn to complex and unusual phase diagrams [7, 8]. Of particular interest are magnetically ordered transition metal oxides, in which a metal-to-insulator (MI) transition as well a magnetic-to-nonmagnetic transition can be tuned by external pressure. In this context, a central issue is what is the impact of those degrees of freedom on the ground state properties when a magnetic insulator is tuned to a nonmagnetic metal across a QCP.

In this respect, the perovskite rare earth nickelates RNiO_3 ($R \neq \text{La}$) are excellent candidates for such studies as they exhibit an insulating antiferromagnetic (AF) ground state: The phase diagram of the RNiO_3 series is shown in Fig. 1. They display a well-defined MI transition at a temperature T_{MI} which increases with decreasing the size of R^{3+} ion ($T_{\text{MI}} = 130 \text{ K}$ (Pr), cc, 600 K (Lu) [9, 10]). Simultaneously the lattice symmetry changes from orthorhombic ($Pbnm$) to monoclinic ($P2_1/n$) which contains two nonequivalent Ni-sites (NiO_6) octahedra with slightly different Ni-O bond lengths, indicating charge disproportionation (CD), $2\text{Ni}^{3+} \rightarrow \text{Ni}^{3+\delta} + \text{Ni}^{3-\delta}$ [11–13].

Another though related interpretation of the phenomena occurring at the MI transition is the important role of oxygen holes [13, 14], which play a very important role in these materials with negative charge-transfer gap [15]. This picture is actually very close to the picture of disproportionation to more and less covalent Ni sites, proposed by Goodenough [16] and in Ref. [17]. As a matter of fact, in reality both these pictures are different sides for the same phenomenon, with the charges on Ni sites more different for smaller rare earths R in the series RNiO_3 , and more equivalent for larger R . Further on we denote both these

pictures as CD.

Recently, resonant x-ray diffraction [18, 19], Raman spectroscopic studies [20] and high resolution x-ray absorption at the Ni K -edge [21] indicate the existence of CD in the whole $R\text{NiO}_3$ series. Moreover, very recent studies on $R\text{NiO}_3$ using soft x-ray magnetic powder diffraction [22] demonstrate that the $R\text{NiO}_3$ compounds have very similar electronic and magnetic states despite the large variation of the value of their T_{MI} .

At low temperatures, the transition to AF ordered state is also related to the size of the R^{3+} ion, i.e. for large R^{3+} ions ($R = \text{Pr}$ and Nd) the MI transition occurs simultaneously with an antiferromagnetic (AF) ordering of the (Ni) sublattice (i.e. $T_{\text{N}} \approx T_{\text{MI}}$), whereas for smaller R^{3+} ($R = \text{Sm} \rightarrow \text{Lu}$) ions, T_{N} is much lower than T_{MI} (e.g. for EuNiO_3 , $T_{\text{N}} = 220$ K and $T_{\text{MI}} = 463$ K). The magnetic structure in the Ni sublattice of $R\text{NiO}_3$ proposed by neutron-powder diffraction [11, 23, 24] has a magnetic propagation vector $\mathbf{k}=(1/2,0,1/2)$ and consists of an up-up-down-down stacking of Ni magnetic moments. An alternative non-collinear magnetic structure with the same propagation vector is recently suggested by resonant soft x-ray magnetic diffraction studies on $R\text{NiO}_3$ [19, 22, 25].

As mentioned above, according to the magnetic phase diagram of the $R\text{NiO}_3$ series at ambient pressure (see Fig. 1), the ground state changes from an antiferromagnetic insulating ($R \neq \text{La}$) to a nonmagnetic metallic state ($R = \text{La}$) through a QCP. Figure 1 shows the phase diagram in terms of the tolerance factor t , which reflects the degree of distortion of perovskites and is determined by ratio of the relative R -O and Ni-O bond lengths, $d_{R-\text{O}}$ and $d_{\text{Ni}-\text{O}}$, $t = (d_{R-\text{O}})/\sqrt{2}(d_{\text{Ni}-\text{O}})$. As the distortion is larger in for small R^{3+} ions, t increases as the radius R^{3+} increases. The figure also shows that t increases with increasing pressure. Regarding the effect of external pressure on T_{MI} and T_{N} in $R\text{NiO}_3$, only few compounds have been investigated up to very high pressure until now, in particular the pressure dependence of T_{N} in them. While the initial change $T_{\text{N}}(p)$ up to about 2.8 GPa reveals a small increase of T_{N} with pressure for $R = \text{Sm}$, Eu and Gd [26], for NdNiO_3 and PrNiO_3 ($T_{\text{N}} = T_{\text{MI}}$) T_{N} is strongly reduced with pressure [27, 28] and even suppressed to zero in PrNiO_3 across a QCP [29]. In the latter case a broad NFL behavior in the vicinity of the QCP has been reported [29].

In this work we study the pressure effect on the structural, transport and magnetic properties of one of perovskite nickelates, EuNiO_3 . We have selected EuNiO_3 ($T_{\text{MI}} = 463$ K and $T_{\text{N}} = 220$ K) which is one of typical $R\text{NiO}_3$ compounds with $T_{\text{MI}} > T_{\text{N}}$ and thereby allows

one to investigate the evolution of the magnetic state under high pressure across a QCP. The presence of ^{151}Eu Mössbauer isotope in EuNiO_3 allows us to realize such an investigation at a microscopic level using the ^{151}Eu nuclear forward scattering (NFS) of synchrotron radiation - a technique based on the Mössbauer effect. The application of the ^{151}Eu NFS technique allows one to probe the magnetic state of the Ni sublattice of EuNiO_3 under pressure via the induced magnetic hyperfine (hf) field at the ^{151}Eu nuclei which results from the ordered Ni magnetic moment. Some preliminary data which demonstrate the applicability of this technique on EuNiO_3 have been published by some of the authors elsewhere ([30], see below). The present ^{151}Eu NFS data on EuNiO_3 , in combination with low temperature synchrotron angle-resolved x-ray diffraction measurements up to about 20 GPa reveal a magnetic QCP at 10.5 GPa. Since the high pressure resistance data on EuNiO_3 reveal a pressure-induced insulator-to-metal (IM) transition at $p_{\text{IM}} \sim 6$ GPa [30], the results suggest that for pressures between 6 and 10.5 GPa the pressure-induced metallic state is magnetically ordered. Similar metallic antiferromagnetic state was proposed in Ref. [31], and recently observed in strained multilayers of $\text{PrNiO}_3/\text{PrAlO}_3$ [32]. The presence of this state can be possibly explained by the picture of spin density wave [33]. As the lattice symmetry in this state in our system remains monoclinic, we suppose that certain CD exist in this case too, although we do not have definite proof of that. We further show from the analysis of the high pressure electrical resistivity data on EuNiO_3 [30] that in different pressure ranges beyond the QCP both NFL and Fermi liquid (FL) regimes are realized.

It is worthwhile to mention that beside RNiO_3 bulk samples, rare earths nickelates are very actively studied nowadays as thin films and multilayers [34, 35]. In particular, one can effectively control their properties by using epitaxial strain (and spatial confinement) induced by the substrate, which is rather similar, but not identical to the pressure effects studied in this paper.

II. EXPERIMENTAL DETAILS

A polycrystalline sample of EuNiO_3 was prepared under an oxygen pressure of 200 bars. Details of the preparation and characterization were published elsewhere [36]. The ^{151}Eu NFS experiments were carried out under pressure and at low temperature using a clamp-type diamond-anvil cell (DAC) on beamline BL09XU at SPring-8. The first excited nuclear

state of ^{151}Eu has an energy of 21.541 keV (resonance energy) and a half lifetime of 9.7 ns. The pulsed synchrotron radiation was monochromatized to a bandwidth of 1.8 meV at the resonant excitation energy of ^{151}Eu nuclei by a high-resolution monochromator. The monochromatized x-ray transmitted through the sample was detected with the stacked Si-avalanche photodiodes. The storage ring was operated in a special bunch mode where the interval between successive single bunches is 165.2 ns which is much longer than the half lifetime of the first excited nuclear state. The powder-samples were loaded with ruby chips into a sample cavity of a 0.5 mm diameter in a 0.2 mm thick Inconel 625 alloy gasket and mixtures of methanol-ethanol as a pressure-transmitting medium to ensure hydrostatic conditions. Pressure was calibrated by measuring the wavelength shift of the R_1 luminescence line of ruby chips in the clamp-type DAC at room temperature.

The x-ray diffraction data were collected under pressure up to approximately 20 GPa at 8 K by the angle-dispersive technique and using an image-plate detector on beamline BL10XU at SPring-8. The incident x-ray wavelength was 0.4153 Å, which was calibrated by measuring the x-ray diffraction pattern of CeO_2 at ambient conditions. The powder-samples were loaded into a He-gas driven DAC with ruby chips and He as a pressure-transmitting medium to ensure hydrostatic conditions. Pressure was calibrated by measuring the wavelength shift of the R_1 luminescence line of ruby chips in the DAC at 8 K.

III. RESULTS AND DISCUSSION

A. High pressure ^{151}Eu nuclear forward scattering

As mentioned above, the ^{151}Eu NFS of synchrotron radiation allows one to probe the magnetic state of the Ni sublattice of EuNiO_3 under pressure via the induced magnetic hf field B_{hf} at the ^{151}Eu nuclei which results from the ordered Ni magnetic moment. B_{hf} originates from the exchange (transferred) field due the admixture of the magnetic (7F_1) excited state into the nonmagnetic (7F_0) ground state. The magnitude of B_{hf} depends both on the size and relative orientation of the Ni moments around the ^{151}Eu nuclei. The first attempt to demonstrate the applicability of this technique on EuNiO_3 has been reported in Ref. [30]. In this work the authors only measured two pressure points (9.5 and 14.4 GPa) and detected no magnetic signal at 14.4 GPa, and thus these preliminary measurements

provided no information about the pressure dependence of T_N or B_{hf} , which is necessary to construct a (p, T) -magnetic phase diagram. In the present work using the high pressure ^{151}Eu NFS technique we performed systematic measurements of the pressure dependences of T_N and B_{hf} of EuNiO_3 and were able to locate the magnetic QCP and thus to construct the (p, T) -magnetic phase diagram of EuNiO_3 .

Figures 2 (a) and (b) show some selected ^{151}Eu NFS spectra at different pressures and temperatures, both in the paramagnetic states (7.3 GPa at 300 K and 10.7 GPa at 5 K) and magnetically ordered state (4.7, 7.3, and 9.7 GPa at 5 K). In all spectra, we observe quantum beats due to electric quadrupole and/or magnetic hf interactions which cause splitting of the nuclear levels and thus lead to a constructive interference of the photons emitted from these energy levels. As seen in Fig. 2 (a), the frequencies of quantum beats in the ^{151}Eu NFS spectra observed below 9.7 GPa at 5 K are higher than those in the spectrum at 10.7 GPa and 5 K. These high frequencies of the quantum beats come from large energy splitting due to magnetic hf splitting of the ^{151}Eu nuclear levels in the magnetically ordered state. In comparison, the feature of low frequency in the ^{151}Eu NFS spectrum on the paramagnetic state at 7.3 GPa and 300 K (Fig. 2 (b)) is similar to that at 10.7 GPa and 5 K shown in Fig. 2 (a). These results suggest that magnetic ordering in EuNiO_3 disappears at 5 K above 10.7 GPa.

The fits to the ^{151}Eu NFS spectra were performed using the program package MOTIF [37], applying the full dynamical theory of nuclear resonant scattering and including the diagonalization of the complete hyperfine Hamiltonian. The spectra at 5 K and 10.7 GPa and at 7.3 GPa and 300 K can be fitted by assuming a pure electric quadrupole interaction, indicating a paramagnetic state in EuNiO_3 at 5 K and 10.7 GPa. However, the ^{151}Eu NFS spectra in the magnetically ordered state at 5 K below 9.7 GPa were impossible to fit by only quadrupole interaction; therefore they were fitted by assuming a combined quadrupole and magnetic hf interactions. In such a case, we have considered the magnetic structure of EuNiO_3 at ambient pressure defined by the magnetic propagation vector $\mathbf{k} = (1/2, 0, 1/2)$ as determined by neutron-powder diffraction [24]. In this magnetic structure, the single Eu site is subdivided into two magnetically nonequivalent Eu sites with the ratio of 1:1. One Eu site is sandwiched between two [111] (in cubic setting) layers with parallel spins, i.e., surrounded by six Ni atoms with spin up and two Ni atoms with spin down, sees a transferred hf field, while the other Eu site is nonmagnetic owing to the cancellation of the

Ni antiparallel sublattice magnetic moments at these Eu sites [24].

As shown in Fig. 2 (a), the ^{151}Eu NFS spectra at 5 K below 9.7 GPa were well fitted by assuming two different Eu sites with the ratio of 1:1, that is, one half of ^{151}Eu nuclei has B_{hf} with both electric quadrupole and magnetic hf interactions, and the other has a small electric quadrupole interaction only. Consequently, these results suggest that the magnetic structure in the Ni sublattice of EuNiO_3 does not change under pressure up to 9.7 GPa. The B_{hf} values refined at 5 K are shown in Fig. 2 (a) as a function of pressure. As seen in Fig. 3 (a), the refined values of B_{hf} gradually increases with increasing pressure up to 7.3 GPa, passes through a maximum around 8 GPa, and then disappears at 10.7 GPa, indicating a suppression of Ni magnetic moments.

To obtain the pressure dependence of T_{N} , we have analyzed temperature dependences of the ^{151}Eu NFS spectra at different pressures on the basis of the fitting procedure (see above). Figure 2 (b) shows that the analytical spectra well reproduce the observed ones within the assumptions given above. The values of T_{N} were evaluated from the temperature dependence of B_{hf} at different pressures $B_{\text{hf}}(T, p)$, using the Brillouin function with $S = 1/2$. Figure 3 (b) shows the values of the pressure dependence of T_{N} . As it is evident from Fig. 2 (b), T_{N} slightly increases with pressure up to about 2 GPa. At higher pressures T_{N} decreases and then collapses at about 10.5 GPa, indicating the collapse of magnetic order of the Ni moments in EuNiO_3 . The initial increase of T_{N} with pressure ($p \leq 2.4$ GPa) is in a good agreement with the data of EuNiO_3 reported from resistivity in Ref. [26] and reflects the localized character of the Ni 3d-states in the insulating phase of EuNiO_3 .

Thus, the ^{151}Eu NFS results reveal that with increasing pressure both B_{hf} and T_{N} disappear at $p_{\text{c}} \approx 10.5$ GPa. Keeping in mind that EuNiO_3 displays the pressure-induced IM transition at $p_{\text{IM}} \approx 6$ GPa [30], this result implies that under pressure the ground state of EuNiO_3 changes from AF insulator to AF metal at p_{IM} and then to a nonmagnetic metal above p_{c} . The impact of this finding on the complexity (p, T)-phase diagram of EuNiO_3 will be discussed in the following sections.

B. High pressure synchrotron angle-resolved x-ray diffraction at 8 K

Figure 4 shows some selected integrated x-ray diffraction patterns of EuNiO_3 under pressure at 8 K. In the inset of Fig. 4 (a), the diffraction line at ~ 18 deg. in the pattern

corresponds to the (224) refraction in the orthorhombic $Pbnm$ structure. This diffraction line may split to two (224) and $(22\bar{4})$ refractions in the monoclinic $P2_1/n$ structure. But, as it is also known from the structural data on NdNiO_3 [18] and PrNiO_3 [21], the monoclinic distortion in rare earth nickelates with larger rare earths is very small and difficult to detect directly. That is why it took long time, and required the use of novel, more sophisticated techniques, to finally establish that also these systems $R\text{NiO}_3$, with larger R ions, have monoclinic structure at low temperatures [18, 19, 21]. The situation is the same in our case: as seen in the inset of Fig. 4 (a), we did not observe the monoclinic distortion in EuNiO_3 within our experimental resolution. All diffraction lines in the x-ray diffraction patterns are labeled with the indices of the orthorhombic $Pbnm$ structure. But these results indicate at least that there is no other pressure-induced structural symmetry change up to ~ 20 GPa at 8 K, within our experimental resolution.

Integrated x-ray diffraction patterns were analyzed with the Rietveld refinement program RIETAN-2000 [38] using the orthorhombic $Pbnm$ structure. In each x-ray diffraction pattern, the regions at $2\theta \sim 7.2, 8.4$ and 12.2 deg. were excluded from the refinement procedure where very weak diffraction lines from impurity phases were observed. All integrated x-ray diffraction lines in the patterns up to ~ 20 GPa gave good fits as shown in Fig. 4. It should be noted that these refinement procedures were used to derive individual atomic coordination parameters in addition to the lattice parameters.

In Fig. 5 (a), we show the pressure dependence of the refined lattice parameters of EuNiO_3 at 8 K. As shown in Fig. 5 (a), the pressure dependences of $a = \sqrt{2}a'$, $b = \sqrt{2}b'$, and $c = 2c'$ exhibit no discontinuity up to $p \leq 10.5$ GPa, indicating within the experimental resolution no structural phase transition at $p_{\text{IM}} \approx 6$ GPa. These pressure variations further reveal that the pressure dependences of a , b and c are quite different. With increasing pressure, the value of b decreases more rapidly than those of a and c and the value of a almost saturates at 10.5 GPa. However, no change of the lattice symmetry is observed.

The linear compressibilities κ of the lattice parameters were estimated to be $\kappa_a = 1.11(2) \times 10^{-3}$, $\kappa_b = 2.52(3) \times 10^{-3}$, and $\kappa_c = 1.20(1) \times 10^{-3}$ GPa^{-1} below 10.5 GPa. The estimated κ value of b is twice larger than those of a and c . Furthermore, the pressure dependences of a and c are different from those at room temperature [30]. The bulk moduli

B below 10 GPa and above 11 GPa were evaluated based on the Murnaghan equation,

$$p = \frac{B}{B'} \left[\left(\frac{V_0}{V} \right)^{B'} - 1 \right], \quad (1)$$

where V_0 is the ambient-pressure volume and B' represents a pressure derivative of B . The solid lines in Fig. 5 (b) represent the best-fitting curves obtained and the B values were refined to be 195(2) and 232(4) GPa below 10 GPa and above 11 GPa, respectively. The B value refined below 10 GPa is comparable with those refined at room temperature [30, 39].

Of particular interest is our finding that no change of the lattice symmetry has been observed in metallic magnetic ground state for $p_{\text{IM}} \cong 6 \text{ GPa} \leq p \leq p_c \cong 10.5 \text{ GPa}$. One possibility is that the monoclinic distortion associated with CD is too weak to be detected by our measurements. But the alternative is that the CD is still preserved to some extent also in the metallic state in EuNiO_3 above 6 GPa. This possibility does not contradict our results of ^{151}Eu NFS in the AF metallic state. In this respect, we want to mention that such an unusual ground state has been predicted in and observed under high pressure in similar compounds orbitally degenerate compounds (e.g. YNiO_3 [31]).

Regarding the observed anomalous pressure dependence of the lattice parameter a for $p \geq p_c \cong 10.5 \text{ GPa}$, it is obvious that the anomaly of a is not related to the pressure-induced IM transition at $p_{\text{IM}} \cong 6 \text{ GPa}$ but rather corresponds to the transition from the antiferromagnetic metallic to a nonmagnetic metallic state at p_c , i.e. at the magnetic QCP of EuNiO_3 . The origin of this anomaly will be discussed in Section C.

C. Magnetic and electronic transitions versus structural parameters

In the following, we would like discuss the structural response to the pressure-induced IM transition and magnetic QCP in EuNiO_3 . In the inset of Fig. 5 (a), we show the pressure dependence of the effective bandwidth W as deduced from the structural parameters, which reveals a significant increase around the pressure-induced IM transition ($p \geq p_{\text{IM}} \cong 6 \text{ GPa}$). W is known to be related to the ligand-to-metal hybridization (effective t_{pd} hopping) and can be described in $R\text{NiO}_3$ compounds in terms of the Ni-O bond length $d_{\text{Ni-O}}$ and the Ni-O-Ni bond angle θ by the relation of $W \sim \cos(\pi - \theta)/d_{\text{Ni-O}}^{3.5}$ [40]. Thus an increase of W implies a corresponding increase of the effective hopping t_{pd} which is expected as the system is tuned to a metallic state. The averaged $d_{\text{Ni-O}}$ and θ values of EuNiO_3 under pressure

were evaluated from the refined lattice and individual atomic coordination parameters to estimate the averaged W value $\langle W \rangle$ under pressure [41]. Obviously the pressure-induced increase of W above the pressure-induced IM transition ($p \geq p_{\text{IM}} \cong 6$ GPa) reflects the onset of the metallic state in EuNiO_3 .

On the other hand, T_{N} is also related to t_{pd} (W) through the perturbation formula for insulators [6]:

$$T_{\text{N}} \sim \mathcal{J} \sim t_{dd}^2 \left(\frac{1}{U_{dd}} + \frac{1}{\Delta + \frac{U_{pp}}{2}} \right), \quad t_{dd} = t_{pd}^2 / \Delta \quad (2)$$

where U_{dd} is the on-site d - d Coulomb interaction energy, t_{dd} the effective dd hopping matrix element, Δ describes the ligand-to-metal charge-transfer energy, and U_{pp} is the Coulomb repulsion of the two holes at the oxygen site. As shown in Fig. 2 (b), the pressure dependence of T_{N} in the insulating phase of EuNiO_3 ($p \leq p_{\text{IM}} \cong 6$ GPa) reveals an increase with pressure up to about 2.4 GPa, followed by a decrease upon approaching the pressure-induced IM transition, whereas $\langle W \rangle$ monotonously increases in the whole insulator phase ($p \leq p_{\text{IM}} \cong 6$ GPa). Such a deviation from a linear correlation between T_{N} and W in magnetic insulators [26] reflects the proximity to a crossover from localized to itinerant electronic behavior in EuNiO_3 above about 2.4 GPa. This is in agreement with the picture proposed by Zhou *et al.* [42] to explain the pressure-induced magnetic properties in the $R\text{NiO}_3$ series.

Now, we would like to provide an explanation of the observed anomalous behavior of the lattice parameter across the QCP at $p_c \cong 10.5$ GPa. The pressure-induced change of the lattice parameter a is governed by two competing mechanisms that act in opposite ways: (i) the decrease of the average Ni-O bond length $\langle d_{\text{Ni-O}} \rangle$ due to compression of the NiO_6 octahedra which leads to a gradual *decrease of* a with pressure; and (ii) the increase of the average Ni-O-Ni bonding angle $\langle \theta \rangle$ which results in a reduction of the tilting of NiO_6 octahedra and thereby an *increase of* a with pressure. We argue that below $p_c \cong 10.5$ GPa the compression of $\langle d_{\text{Ni-O}} \rangle$ (i) is the dominating factor and prevails in the pressure dependence of a , leading to a decrease of a with pressure. However, at and beyond the QCP the compression of $\langle d_{\text{Ni-O}} \rangle$ becomes weaker and comparable to that due to the increase of $\langle \theta \rangle$ (ii). We believe that this could be related to a corresponding change of the magnetoelastic coupling at and beyond the QCP. As a result, the two competing mechanisms become almost equal and compensate each other, causing a nearly pressure independent change of the lattice parameter a for $p \geq p_c \cong 10.5$ GPa. In such a case, one would anticipate melting

of the charge disproportionation in the nonmagnetic metallic state, caused by the increased bandwidth.

D. Suggested (p, T) -phase diagram of EuNiO_3

On the basis of our ^{151}Eu NFS and low temperature synchrotron x-ray data, we would like to propose the (p, T) -phase diagram for EuNiO_3 , shown in Fig. 6. The overall features of the phase diagram can be summarized as follows: at ambient pressure below $T_{\text{MI}} \sim 460$ K the system undergoes a transition from the orthorhombic metallic state to a monoclinic CD insulating state. The insulating CD state exhibits antiferromagnetic ordering below $T_{\text{N}} \sim 220$ K. Under pressure, this AF insulating and CD ground state changes to an AF metallic and CD state at $p_{\text{IM}} \cong 6$ GPa. At higher pressures the system displays a transition to a non-magnetic state at $p_c \cong 10.5$ GPa i.e. QCP. By further increasing pressure beyond the QCP, the system reveals NFL and FL behavior for $10.5 \text{ GPa} \leq p \leq 14.8 \text{ GPa}$ and $15.9 \text{ GPa} \leq p \leq 17.5 \text{ GPa}$, respectively. The identification of NFL and FL regions are based on the analysis of the original low temperature electrical resistance data on EuNiO_3 reported in Ref. [30]. To analyze the electrical resistance data $R_{\text{abs}}(T)$, we used the power-law fitting to $R_{\text{abs}}(p, T)$ of EuNiO_3 in the temperature range between 10 and 45 K with $\Delta R_{\text{abs}}(T) (= R_{\text{abs}}(T) - R_0) \sim T^n$, where $n = 2$ and $1 < n < 2$ for FL and NFL behavior, respectively. As shown in Figs. 7 (a) and (b), the power-law with $n = 1.6$ fits the experimental data fairly well for $p = 11.5, 13.2$ and 14.8 GPa, indicating NFL behavior, whereas $n = 2$ is the best fitting for 15.9 and 17.5 GPa, corresponding to FL behavior. Our finding of a NFL behavior in EuNiO_3 with $n = 1.6$ is similar to that reported from high pressure resistivity data on PrNiO_3 [29]. The authors show in addition that the suppression of the insulating state of PrNiO_3 ($T_{\text{N}} = T_{\text{MI}} \sim 130\text{K}$) above 1.3 GPa is accompanied by a transformation to a NFL phase in which the resistivity varies proportional to T^n with $n = 1.33$ and 1.6 over a broad pressure range. In EuNiO_3 with $T_{\text{N}} \ll T_{\text{MI}}$, we only observe a NFL behavior with $n=1.6$.

IV. SUMMARY

We have investigated the pressure effect up to about 20 GPa on the structural and magnetic properties of the antiferromagnetic insulator rare earth nickelate EuNiO_3 using

low-temperature synchrotron angle-resolved x-ray diffraction and ^{151}Eu nuclear forward scattering (NFS) of synchrotron radiation, respectively. The ^{151}Eu NFS technique allows one to probe the magnetic state of the Ni sublattice of EuNiO_3 under pressure via the induced magnetic hyperfine field at the ^{151}Eu nuclei which originates from the ordered Ni magnetic moments, and thus to investigate the evolution of the magnetic state under high pressure across a quantum critical point. The experimental results can be summarized as follows.

EuNiO_3 shows two transitions: an insulator-to-metal transition at $p_{\text{IM}} \cong 6$ GPa (already reported) and magnetic-to-nonmagnetic transition with a quantum critical point at $p_c \cong 10.5$ GPa. In this context, we would like to refer to the recent observation of similar metallic antiferromagnetic phase in PrNiO_3 strained multilayers [32].

The analysis of the pressure dependence of the structural parameters revealed a significant increase of the effective bandwidth W , which is related to effective t_{pd} hopping, around the pressure-induced IM transition ($p \geq 6$ GPa). However, we did not detect, within the resolution of the x-ray measurements, any anomalies in the lattice parameters at the IM transition at $p_{\text{IM}} \cong 6$ GPa, and have seen only slight change of the bulk modulus at the quantum phase transition at $p_c \cong 10.5$ GPa. This lets us suggest that most probably the charge disproportionation, existing in $R\text{NiO}_3$ in the insulating phase, survives to certain extent also in the metallic phase. Furthermore, we have shown from the analysis of reported high pressure resistance data on EuNiO_3 at low-temperatures that in the vicinity of the QCP the system behaves as non-Fermi-liquid, the resistance behaving as T^n , with $n=1.6$, whereas it becomes a normal Fermi-liquid, $n = 2$, for pressures above ~ 15 GPa. Based on all obtained data we propose the (p, T) -phase diagram for EuNiO_3 , shown in Fig. 6. We feel that the properties of other nickelates of this class might be similar to those revealed here, i.e. they may be representative also for other perovskite nickelates.

ACKNOWLEDGMENTS

The ^{151}Eu NFS and x-ray diffraction experiments under pressure were performed at SPring-8 with the approval of the Japan Synchrotron Radiation Research Institute (JASRI) (Proposal Nos. 2010A1517, 2008B1460, and 2007A1450). M.M.A. and D.K. would like to thank the Deutsche Forschungsgemeinschaft (DFG) for the support through SFB 608. The work of D.K. was supported by the German project FOR 1346 and by Cologne University

within the German Excellence Initiative.

- [1] H. von Löhneysen, M. Sieck, O. Stockert, and M. Waffenschmidt, *Physica B* **223-224**, 471 (1996).
- [2] H. Löhneysen, S. Mock, A. Neubert, T. Pietrus, A. Rosch, A. Schroder, O. Stockert, and U. Tutsch, *J. Magn. Magn. Mater.* **177-181**, 12 (1998).
- [3] J. Custers, P. Gegenwart, H. Wilhelm, K. Neumaier, Y. Tokiwa, O. Trovarelli, C. Geibel, F. Steglich, C. Pepin, and P. Coleman, *Nature* **424**, 524 (2003).
- [4] N.D. Mathur, F.M. Grosche, S.R. Julian, I.R. Walker, D.M. Freye, R.K.W. Haselwimmer, and G.G. Lonzarich, *Nature* **394**, 39 (1998).
- [5] S.S. Saxena, P. Agarwal, K. Ahilan, F.M. Grosche, R.K.W. Haselwimmer, M.J. Steiner, E. Pugh, I.R. Walker, S.R. Julian, P. Monthoux, G.G. Lonzarich, A. Huxley, I. Sheikin, D. Braithwaite, and J. Flouquet, *Nature* **406**, 587 (2000).
- [6] D.I. Khomskii, *Transition Metal Compounds* (Cambridge University Press, 2014).
- [7] M. Imada, A. Fujimori, and Y. Tokura, *Rev. Mod. Phys.* **70**, 1039 (1998).
- [8] E. Dagotto, *Science* **309**, 257 (2005).
- [9] J.B. Torrance, P. Lacorre, A.I. Nazzal, E.J. Ansaldo, and Ch. Niedermayer, *Phys. Rev. B* **45**, 8209(R) (1992).
- [10] M.L. Medarde, *J. Phys. Condens. Matter* **9**, 1679 (1997).
- [11] J.A. Alonso, J.L. Garcia-Munoz, M.T. Fernandez-Diaz, M.A.G. Aranda, M.J. Martinez-Lope, and M.T. Casais, *Phys. Rev. Lett.* **82**, 3871 (1999).
- [12] J.A. Alonso, M.J. Martinez-Lope, M.T. Casais, M.A.G. Aranda, and M.T. Fernandez-Diaz, *J. Am. Chem. Soc.* **121**, 4754 (1999).
- [13] T. Mizokawa, D.I. Khomskii, and G.A. Sawatzky, *Phys. Rev. B* **61**, 11263 (2000).
- [14] S. Johnston, A. Mukherjee, I. Elfimov, M. Berciu, and G. A. Sawatzky, *Phys. Rev. Lett.* **112**, 106404 (2014).
- [15] J. Zaanen, G.A. Sawatzky and J.W. Allen, *Phys. Rev. Lett.* **55**, 418 (1985).
- [16] J.B. Goodenough, *J. Solid State Chem.* **1217**, 126 (1996).
- [17] J.-S. Zhou and J.B. Goodenough, *Phys. Rev. B* **69**, 153105 (2004).
- [18] U. Staub, G.I. Meijer, F. Fauth, R. Allenspach, J.G. Bednorz, J. Karpinski, S. M. Kazakov,

- L. Paolasini, and F. d’Acapito, *Phys. Rev. Lett.* **88**, 126402 (2002).
- [19] V. Scagnoli, U. Staub, A. Mulders, M. Janousch, G. Meijer, G. Hammerl, J. Tonnerre, and N. Stojic, *Phys. Rev. B* **74**, 100409(R) (2006).
 - [20] M. Zaghrioui, A. Bulou, P. Lacorre, and P. Laffez, *Phys. Rev. B* **64**, 081102 (2001)
 - [21] M. Medarde, C. Dallera, M. Grioni, B. Delley, F. Vernay, J. Mesot, M. Sikora, J. A. Alonso, and M.J. Martinez-Lope, *Phys. Rev. B* **80**, 245105 (2009).
 - [22] Y. Bodenthin, U. Staub, U. Piamonteze, M. Garcia-Fernandez, M.J. Martinez-Lope, and J.A. Alonso, *J. Phys. Condens. Matter* **23**, 036002 (2011).
 - [23] J.L. Garcia-Munoz, J. Rodriguez-Carvajal, P. Lacorre, and J.B. Torrance, *Phys. Rev. B* **46**, 4414 (1992).
 - [24] J. Rodriguez-Carvajal, S. Rosenkranz, M. Medarde, P. Lacorre, M.T. Fernandez-Diaz, F. Fauth, and V. Trounov, *Phys. Rev. B* **57**, 456 (1998).
 - [25] V. Scagnoli, U. Staub, Y. Bodenthin, M. Garcia-Fernandez, A.M. Mulders, G.I. Meijer, and G. Hammerl, *Phys. Rev. B* **77**, 115138 (2008)
 - [26] J.S. Zhou, J.B. Goodenough, and B. Dabrowski, *Phys. Rev. Lett.* **95**, 127204 (2005).
 - [27] X. Obradors, L.M. Paulius, M.B. Maple, J.B. Torrance, A.I. Nazzal, J. Fontcuberta, and X. Granados, *Phys. Rev. B* **47**, 12353 (R) (1993).
 - [28] P.C. Canfield, J.D. Thompson, S.-W. Cheong, and L.W. Rupp, *Phys. Rev. B* **47**, 12357 (1993).
 - [29] J.S. Zhou, J.B. Goodenough, and B. Dabrowski, *Phys. Rev. Lett.* **94**, 226602 (2005).
 - [30] R. Lengsdorf, A. Barla, J.A. Alonso, M.J. Martinez-Lope, H. Micklitz, and M.M. Abd-Elmeguid, *J. Phys. Condens. Matter* **16**, 3355 (2004).
 - [31] I.I. Mazin, D.I. Khomskii, R. Lengsdorf, J.A. Alonso, W.G. Marshall, R.M. Ibberson, A. Podlesnyak, M. J. Martinez-Lope, and M.M. Abd-Elmeguid, *Phys. Rev. Lett.* **98**, 176406 (2007).
 - [32] M. Hepting, M. Minola, A. Frano, G. Cristiani, G. Logvenov, E. Schierle, M. Wu, M. Bluschke, E. Weschke, H.-U. Habermeier, E. Benckiser, M. Le Tacon, and B. Keimer, *Phys. Rev. Lett.* **113**, 227206 (2014).
 - [33] S.B. Lee, R. Chen and L. Balents, *Phys. Rev. Lett.* **106**, 016405 (2011).
 - [34] A. Frano, E. Schierle, M. W. Haverkort, Y. Lu, M. Wu, S. Blanco-Canosa, U. Nwankwo, A. V. Boris, P. Wochner, G. Cristiani, H. U. Habermeier, G. Logvenov, V. Hinkov, E. Benckiser, E. Weschke, and B. Keimer, *Phys. Rev. Lett.* **111**, 106804 (2013).

- [35] J. Chakhalian, J.W. Freeland, A.J. Millis, C. Panagopoulos, and J.M. Rondinelli, *Rev. Mod. Phys.* **86**, 1189 (2014).
- [36] J.A. Alonso, M.J. Martinez-Lope, and I. Rasines, *J. Solid State Chem.* **120**, 170 (1995).
- [37] Y.V. Shvyd'ko, *Hyperfine Interact.* **125**, 173 (2000).
- [38] F. Izumi and T. Ikeda, *Mater. Sci. Forum* **321-324**, 198 (2000).
- [39] J.S. Zhou, J.B. Goodenough, and B. Dabrowski, *Phys. Rev. B* **70**, 456 (2004).
- [40] W.A. Harrison, *The Electronic Structure and Properties of Solids* (Freeman, San Francisco 1980).
- [41] Owing to the two crystallographically nonequivalent O sites in $R\text{NiO}_3$ with orthorhombic $Pbnm$ structure, there are two different $d_{\text{Ni-O}}$ values for the NiO_6 octahedron and two different θ values between the NiO_6 octahedra. The averaged $d_{\text{Ni-O}}$ and θ values of EuNiO_3 under pressure were evaluated from the refined lattice and individual atomic coordination parameters to estimate the averaged W value $\langle W \rangle$ under pressure.
- [42] J.-S. Zhou, J.B. Goodenough, and B. Dabrowski, *Phys. Rev. B* **67**, 02040 (R) (2003).
- [43] J.G. Cheng, J.S. Zhou, J.B. Goodenough, J.A. Alonso, and M.J. Martinez-Lope, *Phys. Rev. B* **82**, 085107 (2010).

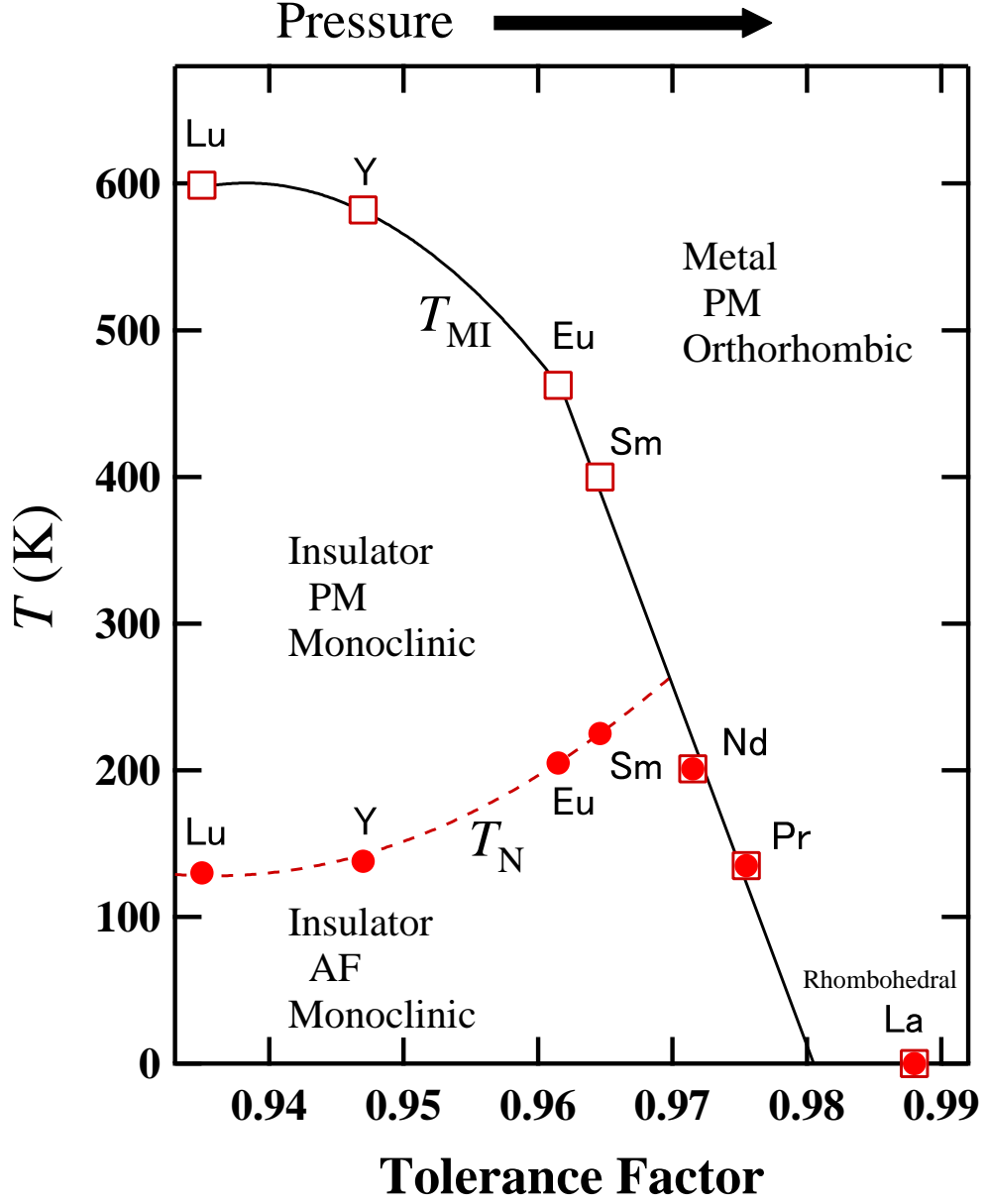


FIG. 1. (Color online) The phase diagram of the $RNiO_3$ series as a function of the tolerance factor t (see text) and external pressure, adapted from data in Refs. [9, 10, 12]. PM and AF stand for paramagnetic and antiferromagnetic, respectively.

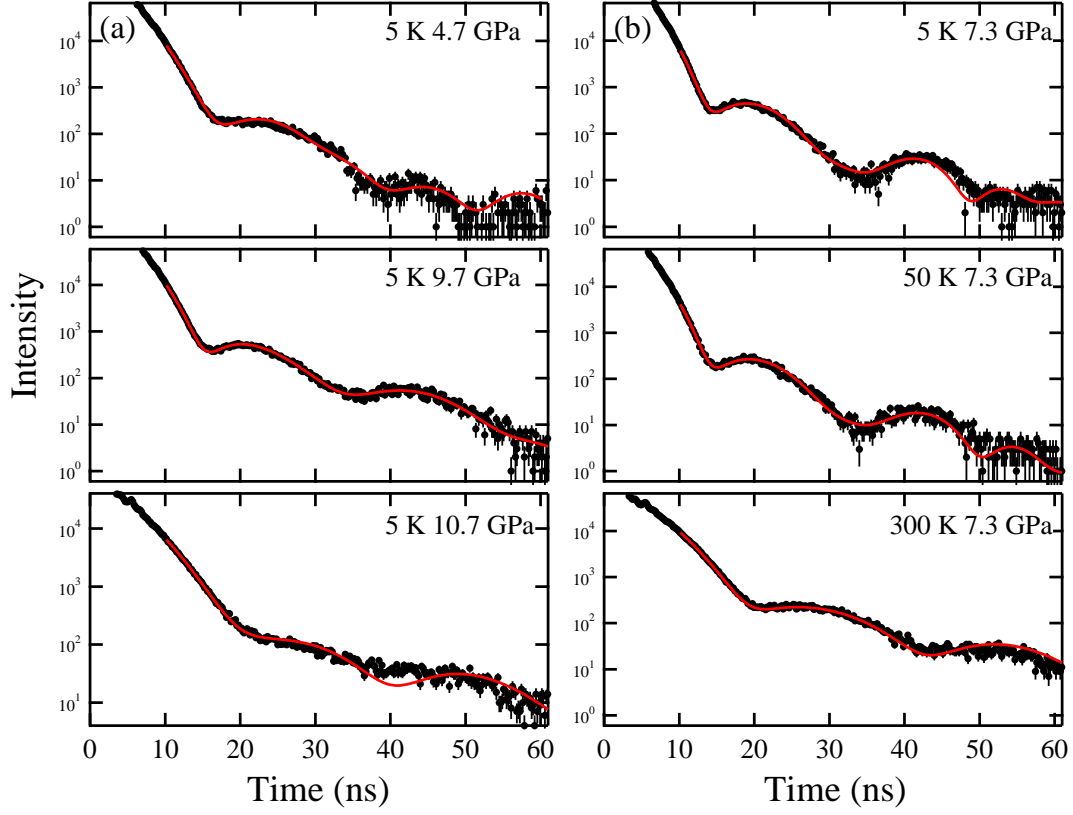


FIG. 2. (Color online) Selected ^{151}Eu nuclear forward scattering spectra of EuNiO_3 (a) at 5 K under pressures and (b) at 7.3 GPa as a function of temperature. The closed circles with error bars indicate the observed spectra and the red solid lines represent the best fitted curves obtained using MOTIF [37].

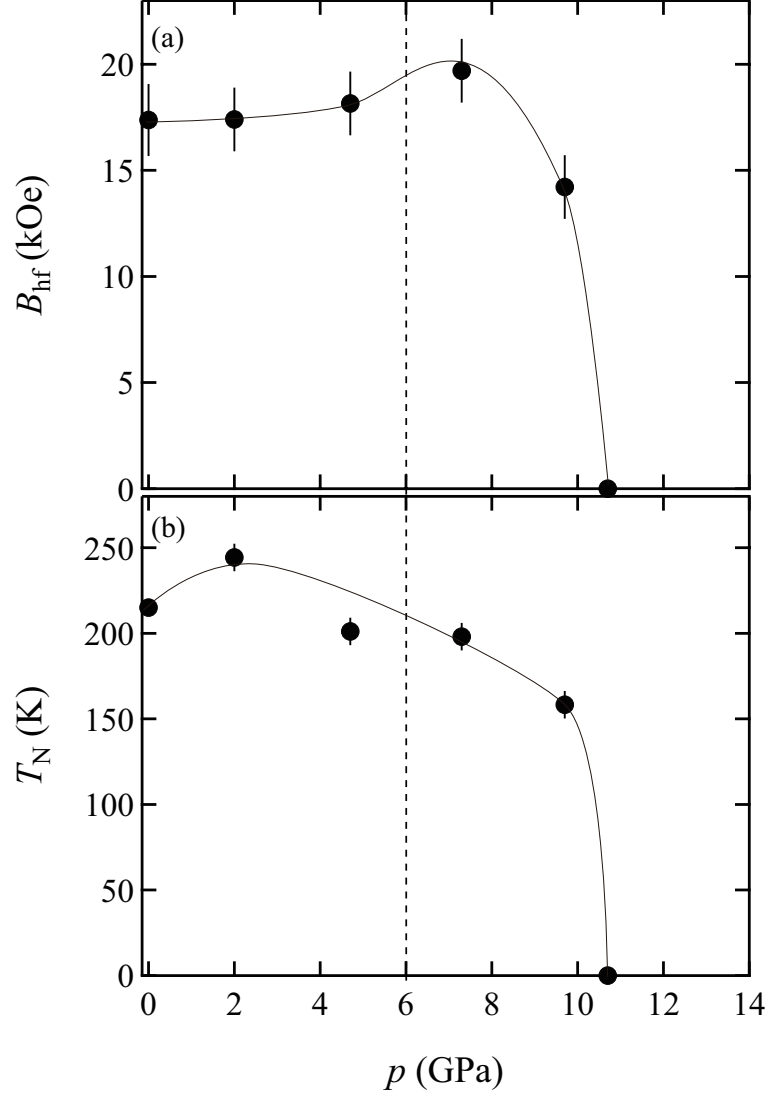


FIG. 3. (a) Refined magnetic hyperfine field B_{hf} at 5 K and (b) evaluated Néel temperature T_N of EuNiO_3 as a function of pressure. At ambient pressure, B_{hf} was refined from the data at 3 K in Ref. [30] using MOTIF [37] by assuming two different Eu sites with the ratio of 1:1. Lines through the data points are only a guide to the eye. The broken lines in (a) and (b) indicate the pressure-induced insulator-to-metal transition at $p_{\text{IM}} \cong 6$ GPa which is taken from the high pressure low temperature resistivity data reported in Ref. [30].

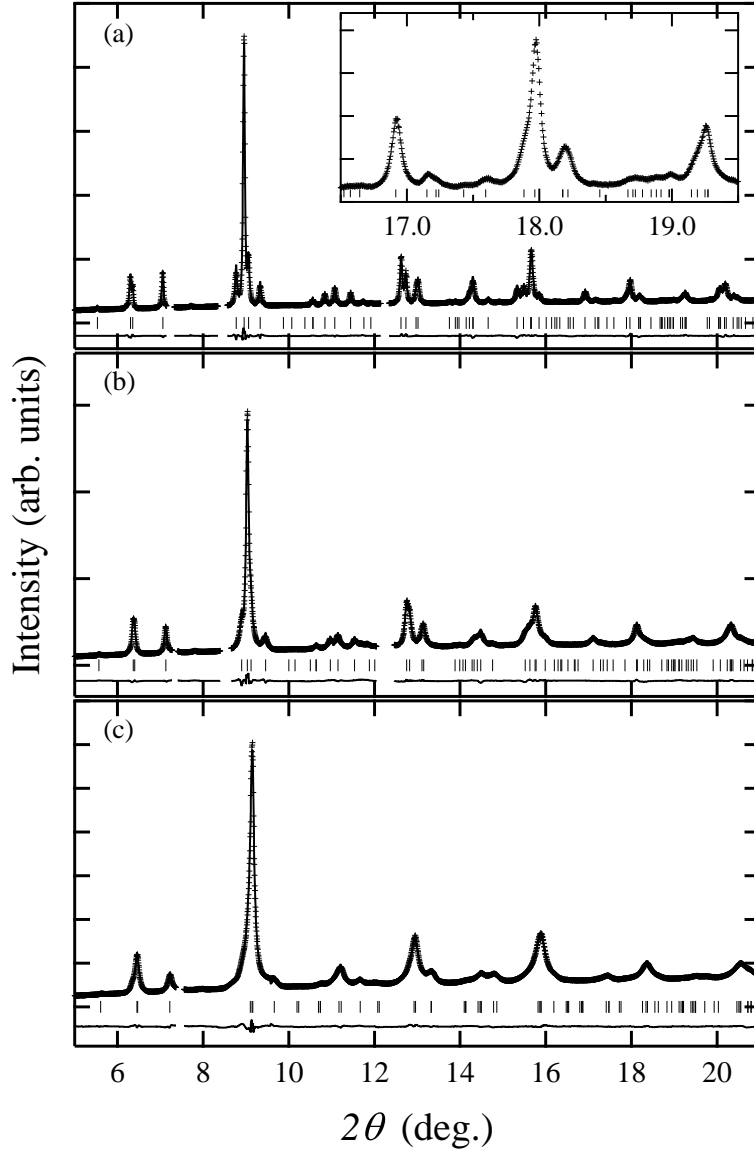


FIG. 4. Selected integrated x-ray diffraction patterns of EuNiO_3 under (a) 2.0, (b) 7.6, and (c) 17.4 GPa at 8 K, where the crosses show the integrated x-ray diffraction intensities. The solid lines represent the results of Rietveld refinement fitting [38] and the tick marks show the positions of all reflections allowed by the orthorhombic $Pbnm$ symmetry. The differences between the integrated and calculated intensities are shown below the tick marks. The inset in (a) shows an enlarged high-angle 2θ region in the pattern at 2.0 GPa, where the effect of monoclinic distortion can be expected.

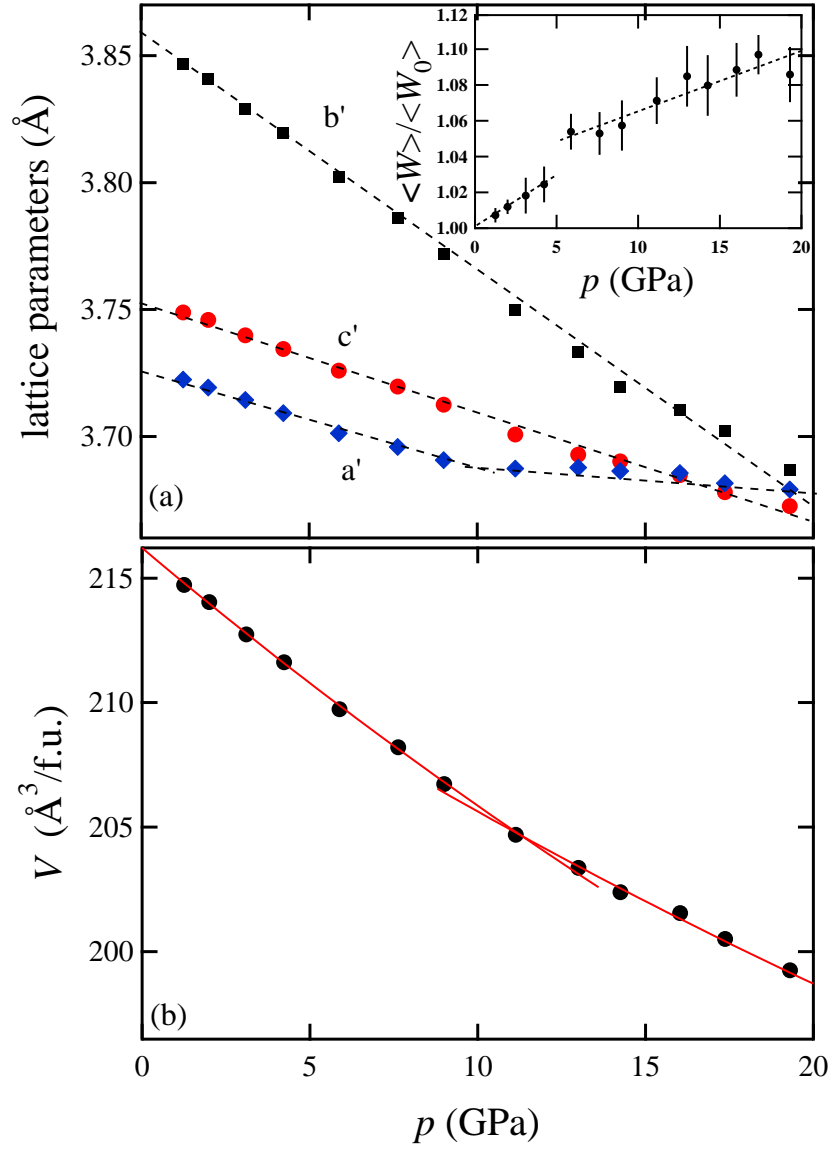


FIG. 5. (Color online) (a) Refined lattice parameters, a , b , and c , ($a = \sqrt{2}a'$, $b = \sqrt{2}b'$, and $c = 2c'$) and (b) evaluated volume, V , of EuNiO₃ at 8 K as a function of pressure. The broken lines in (a) are visual guides. The solid lines in (b) represent the fitting results based on the Murnaghan equation. The inset in (a) shows the pressure dependence of normalized bandwidth $\langle W \rangle / \langle W_0 \rangle$ which was evaluated by the refined lattice and individual atomic coordination parameters under pressure. The broken lines in the inset are visual guides.

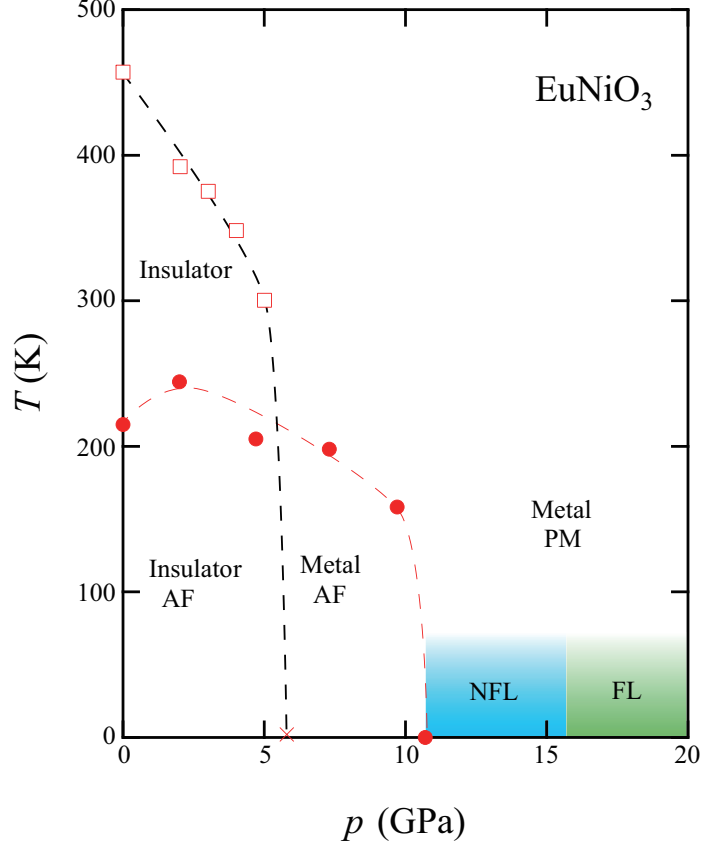


FIG. 6. (Color online) Pressure vs. temperature phase diagram of EuNiO_3 . The closed red circles represent Néel temperature T_N evaluated by present ^{151}Eu nuclear forward scattering data. The open squares indicate the pressure dependence metal-to-insulator transition temperature T_{IM} reproduced from Ref. [43]; extrapolated to the critical pressure (cross point at low temperatures) indicates the pressure-induced insulator-to-metal transition at $p_{\text{IM}} \cong 6$ GPa which is taken from the high pressure low temperature resistivity data reported in Ref. [30]. Non Fermi-liquid (NFL) and Fermi-liquid (FL) regions above 10.5 GPa are identified from the analysis of the original low temperature electrical resistance data on EuNiO_3 reported in Ref. [30].

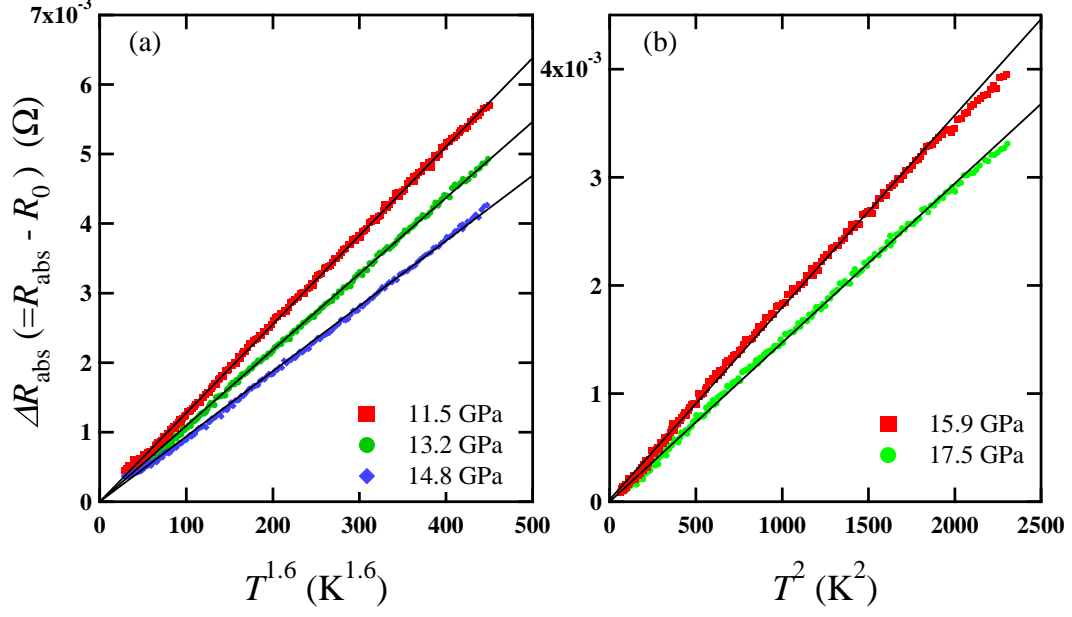


FIG. 7. (Color online) Power-law temperature dependences of electrical resistance R_{abs} in the pressure ranges from 11.5 to 14.8 GPa (a) and from 15.9 to 17.5 GPa (b). The closed symbols indicate the experimental data taken from Ref. [30]. The solid lines represent the fitting results.